Comments on Inorganic Chemistry
Publication details, including instructions for authors and subscription information:
http://www.informaworld.com/smpp/title~content=t713455155

Comments about Cationic-Anionic Redox Competition in the Solid State. The Formation of Anion Associations in the Solid State

Jean Rouxel[a]
[a] Institut des Matériaux de Nantes, UMR CNRS No. 110, Université de Nantes, Nantes Cedex 03, France

To cite this Article Rouxel, Jean(1993) 'Comments about Cationic-Anionic Redox Competition in the Solid State. The Formation of Anion Associations in the Solid State', Comments on Inorganic Chemistry, 14: 4, 207 — 228
To link to this Article: DOI: 10.1080/02603599308048661
URL: http://dx.doi.org/10.1080/02603599308048661

Comments about Cationic–Anionic Redox Competition in the Solid State. The Formation of Anion Associations in the Solid State

JEAN ROUXEL
Institut des Matériaux de Nantes,
UMR CNRS No. 110,
Université de Nantes,
2, Rue de la Houssinière,
F. 44072 Nantes Cedex 03,
France

Received September 16, 1992

The formation of structural entities ranging from anions in simple contacts to true anionic polymers in the solid state is discussed in terms of a competition between d cationic levels and sp anionic ones. Transition metal dichalcogenides, which show two structural domains (layered on the left, tridimensional on the right of the periodic table), provide a wide series of phases to illustrate the process. Polymerization can occur in slabs or from slabs to slabs in the layered structures. Except a few particular cases, like $MnTe_2$, most of the so-called pyrites are also anion-polymerized phases. The electronic transfer, which corresponds to a transfer to the cation of electrons taken from the top of the sp band, may result in the formation of metal–metal bonds. The holes created at the top of the sp band can remain isolated instead of condensing in anionic associations. $CrTe_3$ shows a particular anion–anion exchange which causes the polymerization. Phases like P_xVS_2 or Si_xCrSe_2 are layered phases stabilized by an electronic transfer from the extra elements (Si or P) to the top of the valence band, impeding the formation of anionic associations.

Key Words: *anionic associations, chalcogenides, layered structures, orbital interactions*

Comments Inorg. Chem.
1993, Vol. 14, No. 4, pp. 207–228
Reprints available directly from the publisher
Photocopying permitted by license only

INTRODUCTION

In most solid state chemistry publications, a central role is ascribed to the cationic species in the system under investigation. Crystal structure descriptions are usually based on arrangements of the polyhedra formed by the anions around the cations. We thus speak, for example, of the tetrahedral, octahedral, trigonal prismatic or cubic coordination of a cation.

This point of view is justified by the fact that a compound's constituent cations essentially define its physical properties. Magnetic and optical properties are determined by transition cations with incomplete shells, and cationic levels are often found around the Fermi level whereas the anions contribute bands at lower energies. This leads to an electronic structural description in terms of either a cation-derived conduction band or a correlation between chemical reactivity and the cation's electronic features. When considering redox problems, we in fact refer to the oxidation state of the cation, or at best, to the relative ion stability and electron exchange possible between two cations. The anion is basically characterized by its "bulk" for which no charge fluctuation is envisioned.

The above is perfectly true of the more ionic solids, notably the fluorides and oxides. In these cases, the hard sphere approximation is still valid although orbital interactions may be invoked to account for cooperative magnetic phenomena or deviations from a rigid crystal field model.

When the electronegativity of an anionic species decreases drastically however, a more complex situation may result with the formation of structural entities ranging from anions in simple contact to true anionic polymers. The chalcogenides MX_2 (X = S, Se, Te) of the transition elements provide a remarkable series of compounds permitting a critical description of the redox exchange between anion and cation, and demonstrating the pivotal role of anionic-entity formation vis à vis the structural type and/or the physical properties.

I. MX_2 CHALCOGENIDES: DOMAINS OF STABILITY

It is well known that the transition elements of the left-hand side of the periodic table form layered dichalcogenides while the later

elements of the various periods are associated with the three-dimensional pyrite and marcasite types. Chemically speaking, the determining factor is the destabilization of the higher oxidation states of the cation when moving from the left to the right of the periodic table. Such a destabilization corresponds to a redox competition between cationic d and anionic sp electronic band levels.

Indeed, let us consider a compound from the first, left-hand group, ZrS_2, for example. Its structure (Fig. 1) is based on a stacking of ZrS_2 slabs built from edge-sharing $[ZrS_6]$ octahedra (CdI_2 type). The filled s and p anionic levels form the valence band whereas the corresponding empty cationic levels are pushed towards higher energies. The intermediate metal d orbitals which are split by the crystal field are key to both the structural stability and the physical properties. The classic $t_{2g}-e_g$ splitting occurs (Fig. 2), thus yielding a broad, empty t_{2g} conduction band due to the d^0 configuration of Zr^{4+}. Consequently, ZrS_2 is a diamagnetic semiconductor.

A d^1 configuration in the case of Nb^{4+} lowers the symmetry to a trigonal prismatic one (the slabs now result from an association of NbS_6 trigonal prisms). The d levels are split into a_1' (mostly d_z^2), $e'(d_{xy},\ d_{x^2-y^2})$ and $e''(d_{xz},\ d_{yz})$. As a_1' is lower than the "octahedral" t_{2g} band and is half-populated, this arrangement is energetically favoured[1] and NbS_2 is a metal. MoS_2 and WS_2, which follow immediately within the series, have a d^2 configuration and the same symmetry and are diamagnetic semiconductors (a_1' is filled). Going further to the right, one would expect to recover the octahedral symmetry for a layered MnS_2 for example (no stabilization through a distortion for a d^3 configuration). But this phase does not form. A pyrite is obtained instead. Indeed, as one moves towards the right end of the periodic table, the d level energies decrease progressively and conceivably enough to enter the sp valence band. In such an event, an empty d level will be filled at the expense of the valence band at the top of which holes will appear.[2] In chemical terms, this means that the cation is reduced and the anion oxidized via the formation of anionic pairs. Following this scheme, one goes from layered structures such as TiS_2 with Ti^{4+} and $2S^{2-}$, to pyrites and marcasites with, say, Fe^{2+} and $(S_2)^{2-}$ pairs. Since selenium is less electronegative than sulfur, the top of its sp valence band is situated at a higher energy, and

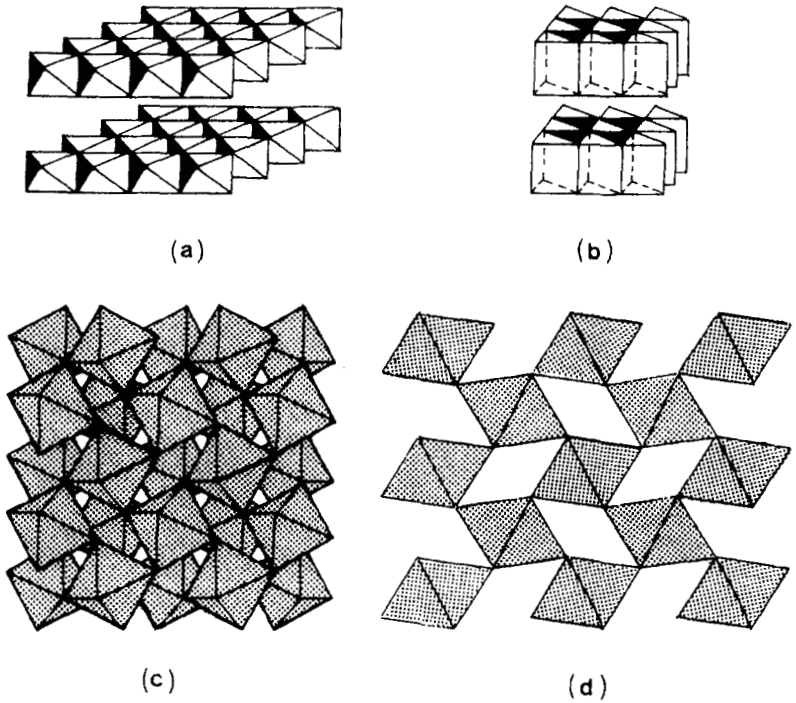

FIGURE 1 The main structural types of transition metal dichalcogenides: (a) layers of sharing edge octahedra (CdI_2 type), (b) layers of trigonal prisms (NbS_2 type), (c) pyrite, (d) marcasite.

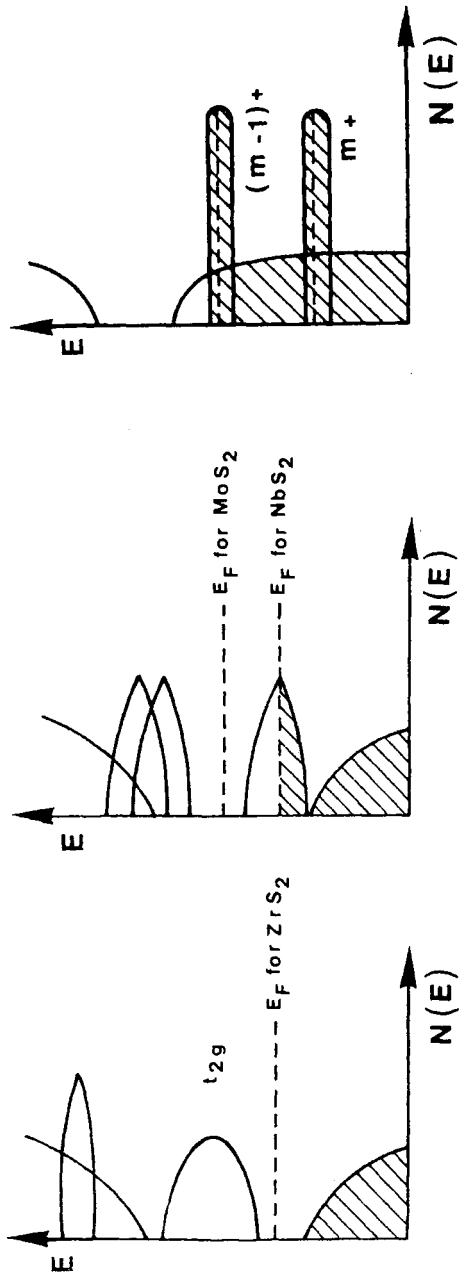

FIGURE 2 Band structure models for layered chalcogenides: (a) ZrS_2, TiS_2, (b) NbS_2, MoS_2; (c) the d levels drop in energy when going to the right of the periodic chart, leading to a lowering of the oxidation state of the cation and the formation of holes at the top of the valence band. The latter can remain isolated or condense into pairs resulting in a pyrite or marcasite structure.

such a transition is observed earlier in the selenides than in the sulfides.

This general model can be considerably improved to explain the subtleties of the structural evolution not only within the layered or 3D pyrite–marcasite type domains, but also at the interface between the two. However, before entering such a critical discussion, it would be worthwhile to consider the soft chemistry processes which allow the stabilization of particular arrangements which are not stable according to the described evolution scheme.

As seen above, a layered MnS_2 compound similar to TiS_2, with octahedral coordination of the metal and a half-filled t_{2g} band, cannot be prepared by direct methods. The lamellar topology and cationic environment anticipated for such a phase can however be attained by adding one electron to MoS_2 with the intercalation of lithium: a phase transition which leads to octahedral molybdenum is observed in $LiMoS_2$.[3] The transformation consists of a simple translation of a sulfide layer relative to the other bounding a [S–Mo–S] slab. Figure 3 shows the pristine host and intercalated compound band schemes which clearly demonstrate the electronic stabilization associated with the transition. It may be pointed out

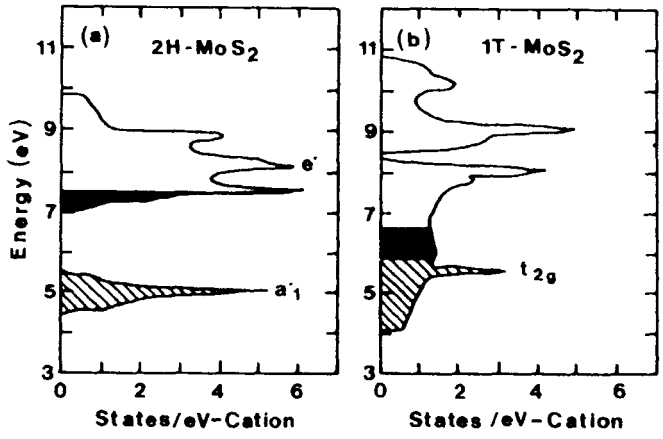

FIGURE 3 Explanation of the formation of an "octahedral" MoS_2. The hatched region corresponds to occupied states in pristine 2H "trigonal prismatic" MoS_2 (left) and in an hypothetical 1T "octahedral" MoS_2. The blackened region shows the additional states filled in 2H-$LiMoS_2$ and 1T-$LiMoS_2$, the latter being the observed structure (after Ref. 3).

that a certain minimum intercalant concentration is required to initiate the transition so that the gain in electronic energy exceeds the cost in the elastic energy entailed by the structural modification. True enough, intercalation usually starts at a critical non-zero value each time a structural alteration, no matter how slight as in the simple shifting of slabs, is involved (compare, for example, Li_xZrS_2 which exhibits a stacking transition and starts at $x \approx 0.25$, and Li_xTiS_2 with its progressive filling of the host's interlayer octahedral sites from $x = 0$).

The driving force for intercalation is thus to be found in that favourable competition between the elastic energy required to modify the host and the gain in electronic energy. In the case being considered, $LiMoS_2$ ($x = 1$) is obtained directly. Non-intercalated MoS_2 persists until enough lithium is provided to achieve the transformation completely. Deintercalating lithium (by electrochemistry or with the use of a mild oxidation reagent like iodine in acetonitrile) would lead to a layered "octahedral" MoS_2 phase. In fact "octahedral" MoS_2 has just been obtained recently when removing potassium from $KMoS_2$ through a chemical route.[4] This implies the presence of strong kinetic constraints which prohibit the recovery of the normally stable trigonal prismatic structure. Similar remarks apply to the formation of lamellar $CrSe_2$ through the deintercalation of lithium from Li_xCrSe_2.[5] In addition, in that case chromium can hardly assume a 4+ oxidation state in a selenium environment. Deintercalation, which is probably incomplete, results in greater oxidation of selenium than of chromium. Holes are created on selenium anions. They may remain isolated on the anions, thus preventing a transition to the pyrite type via the formation of anionic pairs. A metastable layered phase with formula $Li_x^+ Cr^{3+}Se^{2-}Se_{1-x}^{-}Se_x^{2-}$ is probably obtained rather than $Cr^{4+}(Se^{2-})_2$. In the case of the new FeS_2[6] obtained by deintercalation of Li_2FeS_2, the oxidation process concerns sulfur as well as iron. Sulfide anions are oxidized to polysulfide groups and iron is oxidized to Fe^{3+}. The formulation if $Fe^{3+}S^{2-}(S_2)_{1/2}^{2-}$.

II. ANION–ANION INTERACTIONS IN THE LAYERED AND IN THE PYRITE DOMAINS

The normal oxidation state scheme $Ti^{4+}2X^{2-}$ with a broad and empty t_{2g} band leads to the prediction of semiconducting properties

for all the TiX_2 phases. However, while this prediction is correct for TiS_2, both $TiSe_2$ and $TiTe_2$ are metallic. The rising up of the top of the sp band allows an interaction with t_{2g}^7 as shown in Fig. 4. According to Mulliken population analysis, the electronic transfer from the chalcogen to titanium is zero for X = S, very low for X = Se (0.02) but significant for X = Te (0.38) in agreement with bands that are well separated from each other, tangent to each other, or interpenetrating.

This p–d electron transfer is reflected in X–X interchalcogenide distances. Indeed we are depopulating the top of the p block which has some antibonding character. It leads to a shortening of the X–X distances within layers and/or between adjacent layers. For example Te–Te contacts of 3.77 Å are observed in $TiTe_2$ to be compared with the sum of the van der Waals radii (4.00 Å).

Of course, instead of playing with the top of the sp block we can lower, or raise, the position of d levels by substituting a given metal element by another one less, or more, electropositive. The p–d overlap is more important in $TiTe_2$ than in $HfTe_2$, and correlatively the Te–Te contacts are shorter in the former than in the latter. Let us look at the neighbouring columns. One observes at first that the regular hexagonal pattern shown by d^0 Ti^{4+} ions in TiS_2 slabs may be replaced, at least for low-temperature phases, by isolated clusters for d^1 cations[8,9] or simple[10] or complex[11] zig-zag chains for d^2 and d^3 configurations. Then it appears that tellurides may present a particular behaviour. For example V, Nb, Ta ditellurides lead to the formation of double zig-zag chains[12] which represents some intermediate situation between the cluster of d^1 configuration and the d^2 zig-zag chains. It suggests that the formal d electron count for these ditellurides should be $d^{1+\epsilon}$ and not d^1. Calculations have shown this speculation to be correct with, for example, a tellurium to metal transfer of 0.25 electron in the case of vanadium.[13] This situation could be viewed as a transformation of antibonding electrons to bonding ones through an anion to cation transfer. The electrons coming from the top of the sp band with antibonding character are accommodated by the metal through the formation of σ metal–metal bonds, which even results in a further stabilization as compared to the initial metallic levels.

The pyrite structure is usually described as a NaCl modification involving M^{2+} cations and $(S_2)^{2-}$ pairs. Similarly the marcasite

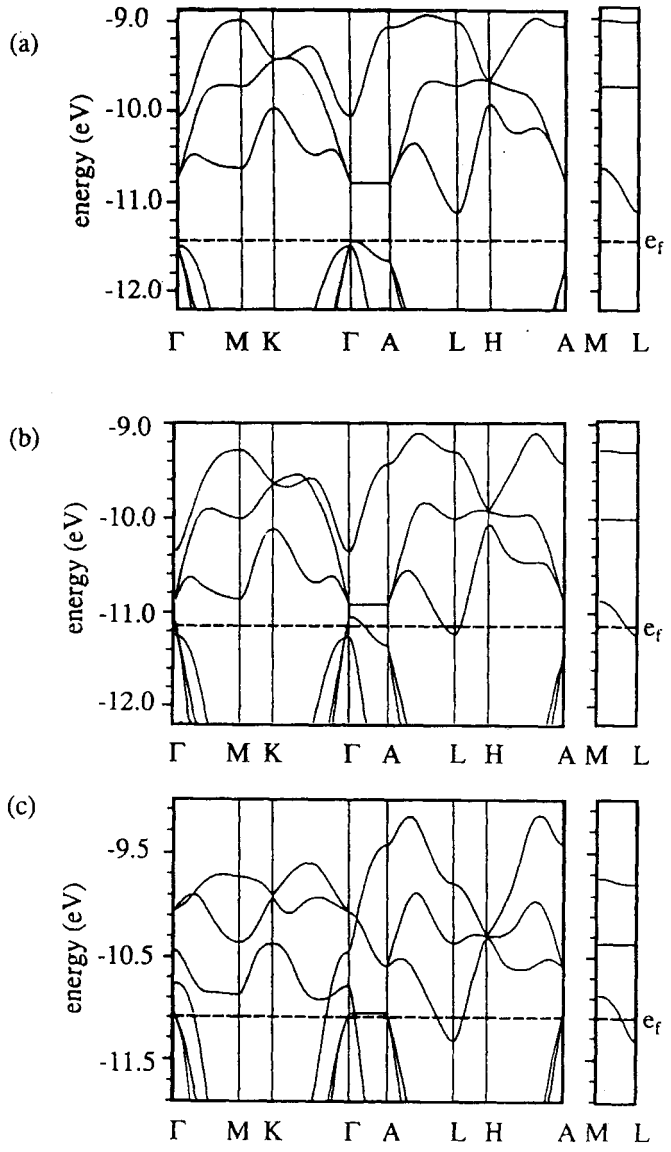

FIGURE 4 Band structures of TiS_2 (a), $TiSe_2$ (b), $TiTe_2$ (c). Dispersion relations, where Γ = (0, 0, 0), M = (1/2, 0, 0), KK = (1/3, 1/3, 0), A = (0, 0, 1/2), L = (1/2, 0 1/2) and H = (1/3, 1/3, 1/2).

can be regarded as deriving from a distorted rutile. The d cationic levels that are to be considered in a pyrite family are the e_g levels which are going to be progressively filled from iron (e_g^0) to zinc (e_g^4). They interact with the last occupied anionic level π^* which is a double level band able to accommodate four electrons (Fig. 5). It results in a bonding band essentially anionic in nature for FeS_2 and an antibonding band with a cationic character.[14,15] However, going to zinc the 3d orbital energy decreases and the bonding band will progressively take a metallic character and the antibonding one a chalcogen-like character. A depletion of the π^* population results, at the beginning, in a strengthening and a shortening of the S–S bond which goes from 2.18 Å in FeS_2 to 2.13 Å in CoS_2, 2.06 Å in NiS_2 and finally 2.03 Å in CuS_2. When copper is reached, the e_g cationic levels are just below π^*, and one electron can be transferred. Copper acquires a d^{10} configuration; the charge

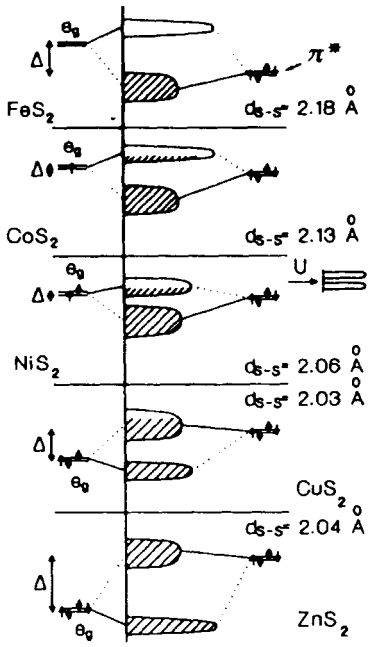

FIGURE 5 Interaction between eg (metal) and π^* (ligand) from Fe to Zn, in pyrites (after Ref. 15).

balance is $Cu^+(S_2)^-$. For ZnS_2, e_g levels are already filled up. The bonding band is completely cationic in character whereas the antibonding one is essentially π^*.

IrS_2, $IrSe_2$[16,17] and $RhSe_2$[18] constitute a small original island inside the pyrite–marcasite domain. The cation is at the 3+ oxidation state. This has been related to the particular stability of the d^6 electronic configuration of the Ir^{3+} and Rh^{3+} cations with low spin configurations in octahedral sites. The associate formulation is $Ir^{3+}S^{2-}(S_2^{2-})_{1/2}$, for example. The structure can be related to a distorted marcasite arrangement, which can be considered as a response of the chalcogen atoms to the very stable oxidation state of the transition metal.

III. ANION-POLYMERIZED STRUCTURES

In the above example anion–anion interactions have been observed, leading eventually to the formation of anionic pairs. This can be regarded as the beginning of an anion polymerization. More complicated species have already been found, for example in Nb_2Se_9 which shows $(Se_5)^{4-}$ anions.[19,20]

With a less electronegative character, i.e., with the top of the sp band at higher energy, tellurium is expected to show the easiest and richest anion–cation redox interactions. Strangely, $IrTe_2$ was reported until recently[21] as exhibiting a CdI_2 layer structure. With the usual configuration, this would mean an Ir^{4+} cation! The same structural type was reported for several other MTe_2 phases and noticeably for $CoTe_2$ and $NiTe_2$, although the disulfides and diselenides of these elements are pyrite and marcasites. One could notice, however, that these phases show an anomaly concerning the cell parameters. Indeed, the *c/a* ratio is equal to 1.37, a much lower value than that reported for usual CdI_2-like ditellurides (ratio $c/a = 1.633$ for ideal hexagonal compact stacking).

Recent structure determination of $IrTe_2$[22] showed that the structure belongs to the P-3m1 space group of CdI_2, but nevertheless presents very particular features with respect to the cadmium iodide arrangement. Indeed short Te–Te contacts are found through the van der Waals gap and also through the structure slabs. A strong decrease in the stacking parameter follows, explaining the

small value of c and the low c/a ratio. Te–Te distances of 3.497 Å and 3.558 Å are found between tellurium ions located at the elevation $z = 1/4$ and $z = 3/4$, on each side of the van der Waals gap, whereas non-bonding anions at the same level are found at 3.928 Å, corresponding reasonably well to the sum of the van der Waals radii (Fig. 6). Integrated atom–atom overlap population calculations at the Fermi level gave positive values, demonstrating the occurrence of Te–Te bonds.[23] $IrTe_2$ is not a layered phase. It is a 3D structure derived from CdI_2, characterized by a polymeric tellurium network. It has been called a polymeric-CdI_2 structure.[24]

With an Ir^{3+} cation, the overall charge on tellurium appears as $(Te_2)^{3-}$. Figure 7 shows a straight-line variation in the Te–Te distances with respect to the anion oxidation states of $(Te_2)^{2-}$ in $MnTe_2$ and $(Te_2)^{4-}$ in $HfTe_2$. The values found in $IrTe_2$ are very close to the ones that would correspond to $(Te^2)^{3-}$ assuming such a linear variation.

A generalization of these results to $CoTe_{2-x}$, a form of $NiTe_2$ (probably $\approx NiTe_{2-x'}$), $RhTe_2$, $PdTe_2$, $PtTe_2$, $CuTe_2$ and $ZnTe_2$

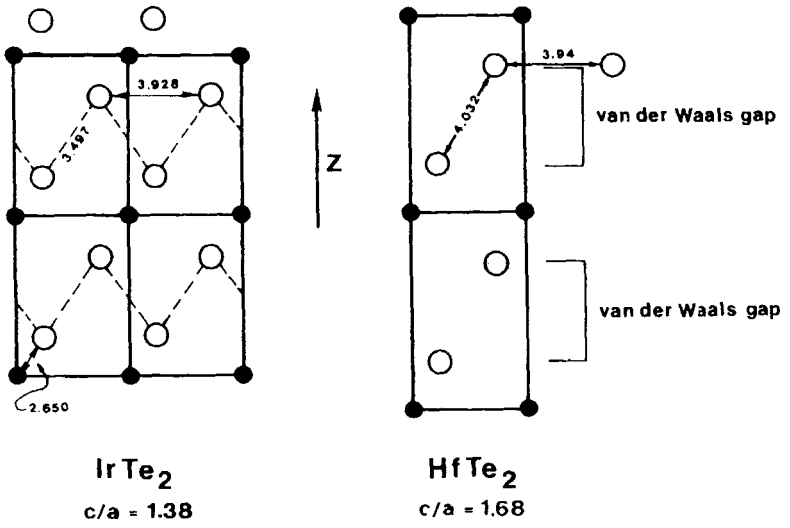

FIGURE 6 Regular CdI_2 structure of $HfTe_2$ (right) and polymerized CdI_2 structure of $IrTe_2$ (left) with short Te–Te contacts through the van der Waals gap reflected in a reduced c/a ratio (1.38 instead of 1.68).

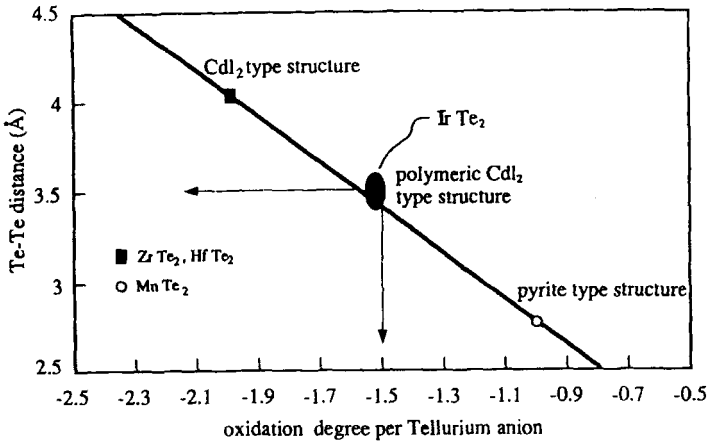

FIGURE 7 Formal oxidation degree per tellurium anion and Te–Te distances in "regular" CdI_2 structural type, pyrite and "polymerized" CdI_2.

can be done. However, an important difference with $IrTe_2$ lies in the expected lower oxidation state for the metal, typically 2+. The cobalt derivatives have been announced as being tellurium deficient ($CoTe_{1.7}$), which is one possible answer to the charge decrease imposed by the cation to the anionic network. In addition, the Te–Te bonding distances are somewhat shorter than in $IrTe_2$, namely 3.483 Å compared with 3.528 Å on average in $IrTe_2$. This is consistent with a decrease in the electronic population of the antibonding levels and a decrease of the formal charge on the Te–Te pairs. However, that decrease is not enough to lead to a charge of -1.2 per tellurium that the formulation $CoTe_{1.7}$ would imply. In fact, the same tellurium to cobalt ratio can be expressed by $Co_{1+x}Te_2$ which makes possible the charge compensation. Such a scheme, also suggested by a c parameter expansion in $CoTe_2$ as compared to other polymeric CdI_2 structures, has been established recently.[25] Table I gives unit cell parameters, interatomic Te–Te distances and associated oxidation states of tellurium in layered CdI_2 and polymeric CdI_2 ditellurides.

$IrTe_2$ is not a true pyrite as discussed just above. There is however an iridium telluride with a pyrite structure. This is Ir_3Te_8 which is metal deficient. The symmetry initially reported to be

TABLE I

Parameters, *c/a* ratios, volumes, interatomic distances and oxidation degrees of tellurium in transition metal ditelluride with CdI_2 and polymeric CdI_2 structure

Compound	$TiTe_2$	$ZrTe_2$	$HfTe_2$	$CoTe_{1/7}$	$RhTe_2$	$IrTe_2$	$NiTe_2$[a]	$PdTe_2$	$PtTe_2$	$CuTe_2$	$ZnTe_2$
a(Å)	3.757	3.950	3.949	3.802	3.92	3.928	3.855	4.037	4.026	3.95	3.98
b(Å)	6.513	6.630	6.651	5.411	5.41	5.405	5.256	5.126	5.221	5.49	5.25
c/a	1.733	1.680	1.68	1.42	1.38	1.38	1.36	1.27	1.30	1.39	1.32
v(Å^3)	79.61	89.58	89.82	67.71	72.0	72.23	67.67	72.33	73.28	74.18	72.02
$d^{(1)}_{Te-Te}$	3.913	4.025	4.032	3.446	3.53	3.498	3.429	3.487	3.464	3.56	3.49
$d^{(2)}_{Te-Te}$	–	–	–	3.521	–	3.558	3.461	3.441	3.526	–	–
$d^{(3)}_{Te-Te}$	3.757	3.950	3.949	3.802	3.92	3.928	3.853	4.036	4.025	3.95	3.98
d_{M-Te}	2.712	2.819	2.822	2.565	2.64	2.650	2.590	2.652	2.676	2.65	2.65
Oxidation States of Te	(<2)	−2	−2	−1.2	−1.5	−1.5	−1.2	(−1.5)	(−1.5)	(<−1)	(−1)
	←	CdI_2	→	←			CdI_2 polymeric				→

$d^{(1)}_{Te-Te}$ refers to interslab Te–Te distances, $d^{(2)}_{Te-Te}$ to anionanion distances belonging to the slab (on both sides of the transition element), and $d^{(3)}_{Te-Te}$ indicates tellurium atoms at the same elevation. The values in parenthese correspond to assumed oxidation states of tellurium.

[a]Probably $NiTe_{1.7}$.

cubic[26] was shown actually to be trigonal[27] with a random distribution of Ir^{3+} on the cationic sites. Te–Te pairs do exist with a d_{Te-Te} distance of 2.833 Å compared with the same bonds in $MnTe_2$, for example (2.75 Å). However, looking at the inter-Te_2-pair distances of the structure, one finds some distances of 3.568 Å, very similar to those found in $IrTe_2$. These distances, much shorter than the sum of van der Waals radii, indicate a bonding between tellurium atoms belonging to different pairs. The result is that we have no longer isolated $(Te_2)^{2-}$ pairs like in true pyrite or $(Te_2)^{3-}$ pairs as would imply the formulation $Ir^{3+}(Te_2)^{3-}$, but each tellurium of a pair is bonded to two others to again form a polymeric

TABLE II

Lattice parameters, volumes (per MTe_2), main interatomic distances and oxidation degrees of tellurium in classical and polymeric MTe_2 pyrite structures

Compounds	Parameters (Å)	Volume per MTe_2 (Å^3)	D_{Me-Te} (Å)	D_{Te-Te} (Å)	Oxidation State of Te
$MnTe_2$	6.951	83.95	2.907	**2.750** 3.955 4.262	−1
$FeTe_2$[a]	6.294	63.32	2.619	**2.626** 3.547 3.855	<-1
$NiTe_2$[a]	6.374	64.75	2.653	**2.650** 3.592 3.904	<-1
$CuTe_2$[a]	6.605	72.05	2.749	**2.746** 3.722 4.046	(?)
$RuTe_2$	6.391	65.25	2.648	**2.790** 3.567 3.914	<-1
$RhTe_2$	6.448	67.02	2.659	**2.696** 3.560 3.951	−1.5
$OsTe_2$	6.397	65.45	2.647	**2.830** 3.561 3.918	<-1
Ir_3Te_8	6.411	65.88	2.653	**2.883** 3.568 3.926	−1.1

Bold and underlined figures relate to the Te_2 pairs and the Te–Te interaction interpairs, respectively.

[a]Distances calculated with a classical fractional coordinate x value of 0.38 for tellurium atoms.

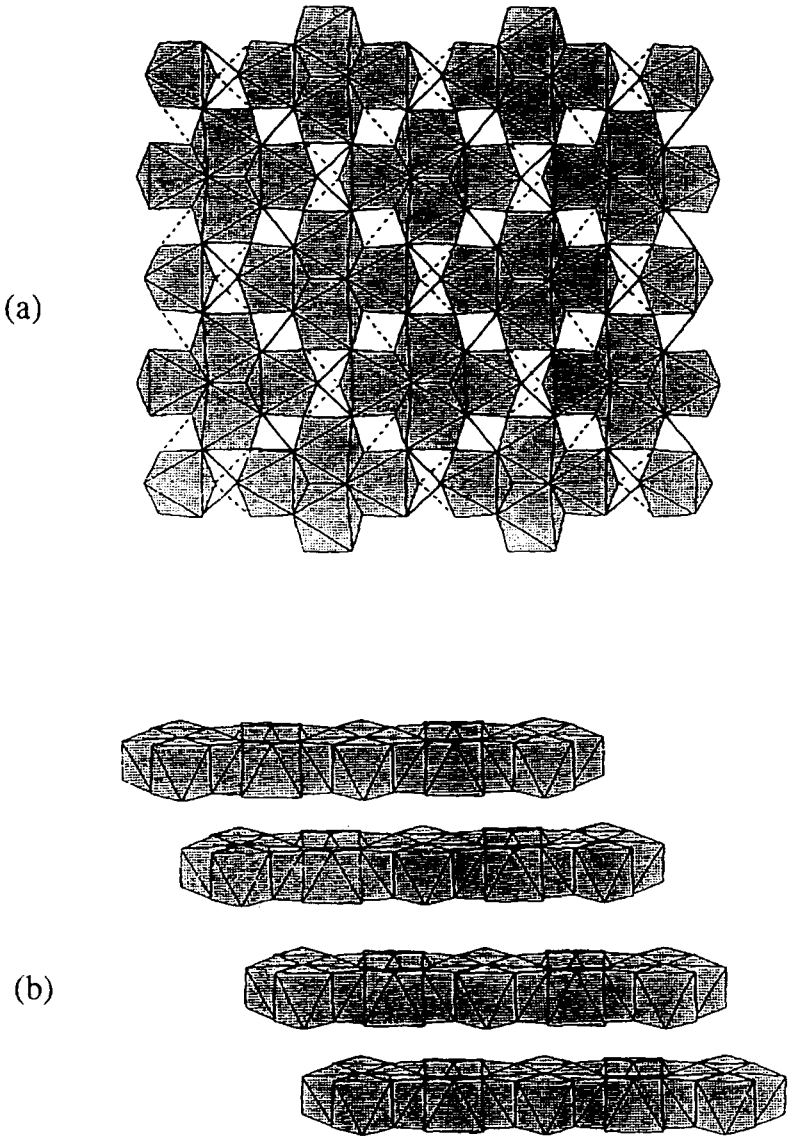

FIGURE 8 (a) layers (b, c plane) of the structure of $Cr_{2/3}Te_2$. They are built up from groups of four edge-sharing octahedra linked through apical tellurium and Te–Te or Te–Te–Te associations; (b) perspective drawing of the layers. There are no Te–Te bonds between successive $Cr_{2/3}Te_2$ layers.

tellurium network with an average charge of -1.1 per tellurium atom.

Finally a survey (Table II) of reported pyrite-like telluride structures[28,29] shows that all phases, with the interesting exception of $MnTe_2$, present such a polymeric pyrite-type structure with very short, medium, and long Te–Te distances corresponding, respectively, to pairing, bonding and non-bonding tellurium anions. This is directly reflected in the unit cell volumes which jump from about 65 Å^3 per molecular weight for the polymeric compounds to almost 84 Å^3. In addition, the tellurium–tellurium pair bond length varies in the series from $MnTe_2$ to $NiTe_2$ and suggests a lowering of the oxidation state on the cation. One might use the same mechanism as the one given for the MS_2 pyrite series from FeS_2 to ZnS_2 to explain the variation of the elongation of the telluirum pairs and of the oxidation state of the cation (<2). The effective charges announced elsewhere,[30] i.e., +2 in $FeTe_2$, +3 in $CoTe_2$ and +4 in $NiTe_2$ are very unlikely and unrealistic.

$CrTe_3$ is another interesting transition metal telluride to be discussed in the same general framework, because, as we shall see below, it can be formulated as $Cr_{2/3}Te_2$. The structure[31] shows a layered arrangement built up from groups of four edge-linked $CrTe_6$ octahedra which are connected via apical tellurium atoms (Fig. 8). In this phase, very stable Cr^{3+} imposes a mean oxidation state of -1 on the tellurium anions and the compound charge balance can be viewed as follows: $[Cr^{3+}]_2[Te^{2-}][Te_2]^{2-}[Te_3]^{2-}$. To the polyanions correspond interatomic distances of 2.816 Å and 2.824 Å for $[Te_3]$ and 2.817 Å for $[Te_2]$. These are a bit longer than expected, which would lead to higher charges on tellurium if these groups were really isolated. In fact, inside sheets, Te–Te distances of 3.437 Å and 3.507 Å are observed, which indicates the presence of bonding. From plane to plane distances of 3.85 Å, close enough to the sum of the van der Waals radii, exclude any bonding. Cr_2Te_3 is a case of a layered structure with in-plane anionic polymerization.

CONCLUSION

A close examination of the interanionic distances in the dichalcogenides reveals a large number of situations ranging from non-

interaction to complete polymerization of the anions. The conventional division between lamellar structures to the left of the periodic table and pyrites and marcasites to the right must then be elaborated to include the formation of new arrangements determined by the direction of the anion–anion interactions. These effects certainly become more pronounced as the anion becomes less electronegative, i.e., when the sp band is at a higher energy.

Figure 9 shows a classification taking into account the phase dimensionality (2D or 3D) and the degree of polymerization within each domain, i.e., the number of directions in which bonding creates polymeric networks. $ZrTe_2$ and $HfTe_2$ represent true layered CdI_2 type structures. Within this 2D domain polymerization can involve each Te layer of the [TeMTe] slabs (in plane polymerization) or it can take place between both tellurium layers (through-slab polymerization). Finally bonding through the van der Waals gap transforms a 2D structure into a 3D arrangement (although a structural description can still be formally based on a layer arrangement). Each situation can exist alone or combined with the others. $Cr_{2/3}Te_2$ is a case of polymerization within the layer. WTe_2 and $MoTe_2$ show in-plane and through-slab polymerization. $TiTe_2$ exhibits a through-van der Waals polymerization, but $IrTe_2$, $Co_{1+x}Te_2$ combine with a through-slab polymerization.

In the 3D domain, true pyrite-like phases ($MnTe_2$ with no polymerization) may lead to polymeric phases like $FeTe_2$, $NiTe_2$, $RuTe_2$, etc.

$CrTe_3$ is particularly interesting. Polymerization does not modify the Cr^{3+} oxidation state. The creation of weak additional bonds in the slabs compensates for the lengthening of the initial normal bonds in the $(Te_2)^{2-}$ and $(Te_3)^{2-}$ polyanions. It is an anion–anion process and not a d–sp competition.

The behaviour of anions in the polymeric CdI_2 structure is, to some extent, symmetrical to that exhibited by cations in true CdI_2 arrangements. With d^1, d^2, d^3 configurations, cationic associations are formed. Likewise, considering $(S_2)^{3-}$ hypothetical and isolated groups, one would have a configuration with a single electron which is rather unstable although it can be observed in the case of $RhSe_2$. In the case of the more electronegative sulfur, stability is often reached through either disproportionation (S^{2-} and $(S_2)^{2-}$) as in IrS_2-type phases. On the other hand, less electronegative tellurium

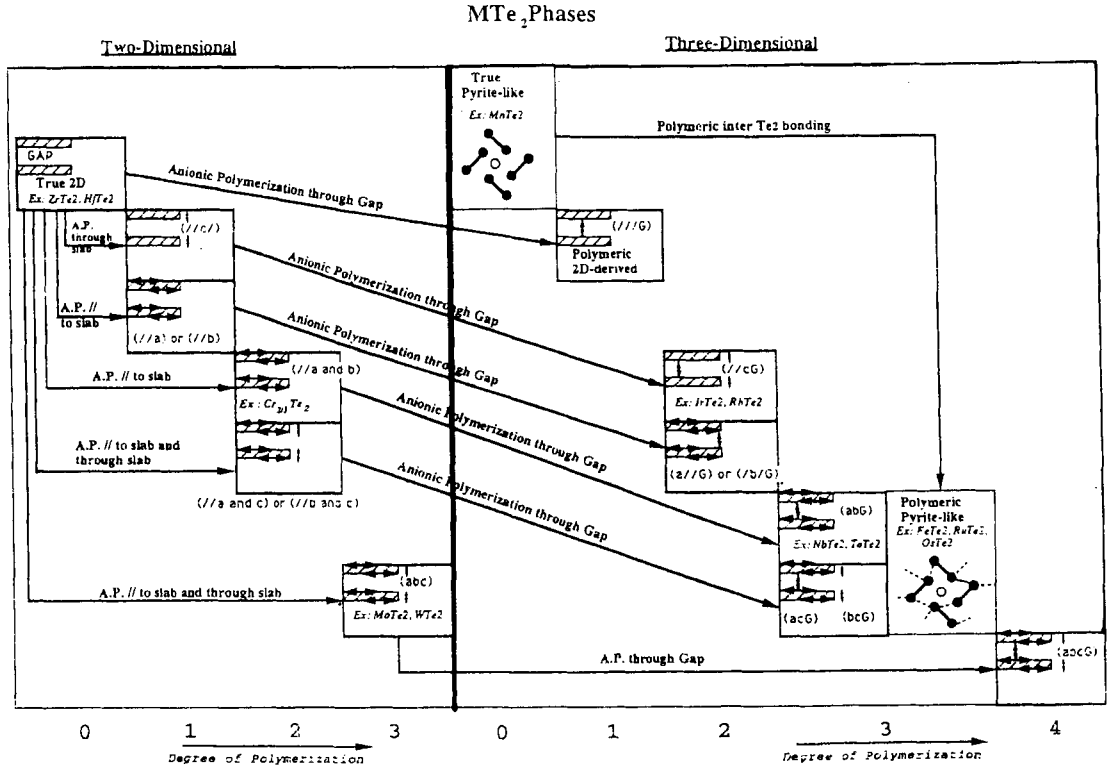

FIGURE 9 Evolution of layer or pyrite types of transition metal ditellurides according to the anionic polymerization degree. Starting from a layered arrangement one can have in-plane polymerization (parallel to slab with two possible a and b directions), through-slab polymerization (c) and through-van der Waals gap polymerization (G), which gives four different polymerization degrees.

allows the setting up of a polymeric network that maintains the same oxidation state on the anions $(X_{2n})^{-3n}$ as in $IrTe_2$-type compounds.

The transition from 2D structures to pyrites and marcasites is related to the pumping of electrons at the top of the sp anionic levels by an empty d cationic level. This could be avoided by reinjecting electrons at the top of the valence band by a third component (Fig. 10). This is probably the explanation of the formation of a Si_xCrSe_2 phase which retains $CrSe_2$ octahedral slabs although chromium is at the 3+ oxidation state. Silicon atoms occupy interstitial tetrahedral holes.[32] The same explanation holds concerning the stabilization of a layered VS_2 arrangement by phosphorus in P_xVS_2.[33]

Binary transition metal dichalcogenides have been considered in this paper. Most of the conclusions could be extended to other chalcogenides. We have pointed out the very transparent behavior of tellurium. No doubt, the very rich chemistry of ternary tellurides which has been developing for the past few years will bring interesting new insights (see, for example, Refs. 34–36 and references there in).

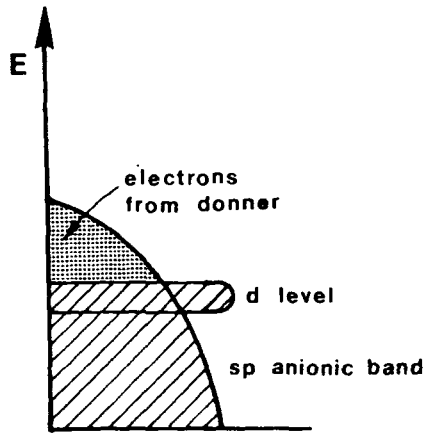

FIGURE 10 Injection of electrons to prevent anionic oxidation and polymerization (Si_xCrSe_2, P_xVS_2).

References

1. R. Huisman, R. de Jonge, C. Haas and F. Jellinek, J. Solid State Chem. **3**, 56 (1971).
2. F. Jellinek, in *Inorg. Sulfur Chemistry*, ed. G. Nickless (Elsevier, Amsterdam, 1968).
3. M. A. Py and R. R. Haering, Can J. Phys. **61**, 76 (1983).
4. R. Schöllhorn, Materials Chemistry (in press).
5. G. A. Wiegers, Physica B **99**, 166 (1980).
6. L. Blandeau, G. Ouvrard, Y. Calage, R. Brec and J. Rouxel, J. Phys. C: Sol. State Phys. **20**, 4271 (1987).
7. E. Canadell, S. Jobic, R. Brec, J. Rouxel and M. H. Whangbo, J. Sol. State, Chem. (in press).
8. J. A. Wilson, F. J. Di Salvo and S. Mahajan, Adv. Phys. **24**, 111 (1975).
9. R. Brouwer and F. Jellinek, Physica B **99**, 51 (1980).
10. (a) E. Canadell and M. H. Whangbo, Inorg. Chem. **29**, 1398 (1990). (b) B. E. Brown, Acta Cryst. **20**, 268 (1966). (c) A. Meerschaut, M. Spiesser, J. Rouxel and O. Gorochov, J. Sol. State Chem. **31**, 31 (1980).
11. (a) N. W. Alcock and A. Kjekshus, Acta Chem. Scand. **19**, 79 (1965). (b) J. C. Wilderwanck and F. Jellinek, J. Less Common Met. **24**, 73 (1971). (c) E. Canadell, A. La Beuze, M. A. El Khalifa, R. Chevrel and M. H. Whangbo, J. Am. Chem. Soc. **111**, 3778 (1989).
12. (a) K. D. Bronsema, G. W. Bus and G. A. Wiegers, J. Sol. State Chem. **53**, 415 (1986). (b) B. E. Brown, Acta Cryst. **20**, 264 (1966).
13. E. Canadell, S. Jobic, R. Brec, J. Rouxel and M. H. Whangbo, J. Sol. State Chem. (in press).
14. C. F. Van Bruggen, Ann. Chim. Fr. **7**, 171 (1982).
15. J. C. W. Folmer, F. Jellinek and J. H. M. Calis, J. Sol. State Chem. **72**, 137 (1988).
16. L. B. Baricelli, Acta Cryst. **11**, 75 (1958).
17. S. Jobic, P. Deniard, R. Brec, J. Rouxel, M. C. B. Drew and W. J. F. David, J. Solid State Chem. **89**, 315 (1990).
18. F. Hulliger, Nature **204**, 644 (1964).
19. A. Meerschaut, L. Guémas, R. Berger and J. Rouxel, Acta Cryst. B **35**, 1747 (1979).
20. S. A Sunshine and J. A. Ibers, Acta Cryst. C **43(6)**, 1019 (1987).
21. E. F. Hocking and J. F. White, J. Phys. Chem. **64**, 1042 (1960).
22. S. Jobic, P. Deniard, R. Brec, J. Rouxel, A. Jouanneaux and A. Fitch, Z. Anorg. Allg. Chem. **199**, 598 (1991).
23. S. Jobic, R. Brec and J. Rouxel, J. Sol. State Chem. **96**, 169 (1992).
24. S. Jobic, R. Brec and J. Rouxel, Journal of Alloys and Compounds **178**, 253 (1992).
25. K. O. Klepp and K. L. Komarek, Monatshefte für Chemie **104**, 105 (1973).
26. A. Kjekshus, T. Rakke and F. A. Andersen, Acta Chem. Scand. A **33**, 719 (1979).
27. S. Jobic, M. Evain, R. Brec, P. Deniard, A. Jouanneaux and J. Rouxel, J. Sol. State Chem. **95**, 319 (1991).
28. G. Brostingen and A. Kjekshus, Acta Chem. Scand. **24**, 2992 (1970).
29. O. Sutarno, Knopp and K. J. G. Reid, Can. J. Chem. **45**, 1991 (1967).

30. H. Binezycka, S. S. Hafner, G. Mohaud and J. Stavek, Phys. Lett. A **145**, 467 (1990).
31. E. Canadell, S. Jobic and R. Brec, Inorg. Chem. (in press).
32. D. Odink, G. Ouvrard and J. Rouxel (to be published).
33. G. Ouvrard, R. Brec and J. Rouxel, Ann. Chim. Fr. **7**, 53 (1982).
34. E. W. Liimatta and J. A. Ibers, J. Sol. State Chem. **71**, 384 (1987).
35. A. Mar and J. A. Ibers, J. Sol. State Chem. **97**, 366 (1992).
36. A. Mar and J. A. Ibers, J. Chem. Soc. Dalton Trans. **536**, (1991).